

X-RAY IMAGING OF FLARE LOOPS AND CORONAL ARCHES

(Invited)

Zdenek Svestka

Laboratory for Space Research, Utrecht, The Netherlands

ABSTRACT

This paper summarizes HXIS results related to preflare, flare-decay, and post-flare phases in the solar corona. Particularly discussed are miniflares, long-lived X-ray enhancements along filament channels, flare precursors (some signifying the flare position, others possibly related to the onset of mass ejections), growth of post-flare loops, images of sites of field-line reconnections late in the flare development, giant post-flare coronal arches with energy contents comparable to coronal transients, and hot loops interconnecting active regions. The extremely low HXIS background, in particular, made it possible to discover many new, previously unknown features in the solar corona. Also emphasized are some problems that have appeared during the evaluation of HXIS data, for the benefit of those who plan future hard X-ray imaging experiments.

I. INTRODUCTION

The original aim of HXIS was an imaging of sources of hard X-ray bursts during the impulsive phase of flares. From the previous talk you could see and judge how well this task has been accomplished. During the eight months of its operations, however, HXIS was able to image many other phenomena of the active Sun in the energy range of 3.5 to 30 keV, and these additional results are the topic of my talk.

Only the two highest energy channels of HXIS, 5(16-22 keV) and 6(22-30 keV) really image hard X rays. The channels 3(8.0-11.5 keV) and 4(11.5-16 keV) represent intermediate energies, and the lowest two channels, 1(3.5-5.5 keV) and 2(5.5-8.0 keV), image soft X-ray emission from the Sun. However, it is important to realize that even the softest HXIS images are by almost one order of magnitude harder than the soft X-ray images of the Sun made on-board the Skylab. Thus, even in soft X rays, HXIS has been able to yield essentially new information about many active phenomena on the Sun.

One of the great advantages of HXIS has been its extremely low background which made it possible to integrate X-ray fluxes for tens of minutes and eventually during the whole (up to 60 min-lasting, sun-lit) orbit if necessary. Table I (Schadee et al., 1983) demonstrates how extremely weak X-ray fluxes can be imaged with statistical significance better than 3σ in the HXIS band 1 for different integration times.

Since the background is the same for every pixel, and the area of one pixel of the coarse field of view of HXIS equals the areas of 16 pixels in the fine field of view, this advantage could be used particularly well in the coarse field. It led to discoveries of completely new structures in the solar corona, undetectable in the high-background Skylab pictures at lower energies. These discoveries were not at all expected when HXIS was launched and are an extra product of the excellent performance of this instrument (for its description cf. Van Beek et al., 1980).

There are many more excellent characteristics of HXIS; for example, its relatively high spatial resolution of 8 arc s in the fine field of view which, after deconvolution (J. Schrijver in Svestka et al., 1984) could be still greatly improved for point-like sources; the capability of HXIS to record X-ray flux variations within each individual pixel, which made it possible to study velocity fields in flares (De Jager, 1985) and in post-flare corona (Svestka, 1984b), among others; the possibility to construct temperature maps of the solar corona which, for example, have led to the detection of rising thermal waves after two-ribbon flares (Svestka, 1984a; Svestka and Hick, 1985).

Nevertheless, and quite naturally, HXIS also had deficiencies. Since this Workshop aims at the preparation of future X-ray-imaging instruments, I consider it particularly important to mention all these deficiencies carefully and in full detail, since one can learn a lot from them. Therefore, while presenting the HXIS results, I will also emphasize all the difficulties and problems we have met when evaluating the data. While doing it, however, I ask the reader to kindly keep in mind that HXIS was an excellent instrument, one of the best flown onboard the SMM; let me, on behalf of all those who have benefitted (and will still benefit) from its data, congratulate Frank van Beek and his co-workers on the invention and construction of HXIS, and the Principal Investigator, Kees de Jager, on its performance and on the fruitful evaluation of HXIS data.

II. POST-FLARE LOOPS

The most important class of flares (since essentially all major flares belong to it) is the two-ribbon flare: two bright ribbons in the chromosphere as the site of footpoints of an arcade of loops which extend high into the corona. New higher loops are sequentially excited, or formed, in the corona, and at the same time their footpoints (the chromospheric ribbons) gradually separate.

This class of flares has been known for about three decades, from $H\alpha$ observations. However, the "post-flare loops" seen in $H\alpha$ are only the cooled remnants of the hot coronal loops, formed (or excited) minutes or tens of minutes before. The enormous advantage of X-ray observations is that we image here the new hot loops close to the time of their excitation or formation and can thus directly study the process of the heating of the loops (energy release) in the corona.

Figure 1 shows in its upper part HXIS images of the system of growing flare loops on 21 May 1980 – this is the flare where Hoyng et al. (1981) first gave the evidence of two hard X-ray footpoints during the impulsive phase (cf. the preceding talk by De Jager). The flare location was in the SW sector of the Sun so that the gradual extension of the X-ray emission to the south means a growth of the flare loops (brightest at the top) upwards in the corona (Svestka et al., 1982a).

At the bottom of Figure 1 we show the growth of the distance d of the brightest portion of the loops from the $H_{\parallel} = 0$ line (Svestka and Poletto, 1985). For radial loops the real altitude would be $3.0 d$. One can see that the growth of the flare loops in altitude was not continuous: the tops of the loops stay for minutes at a given altitude before, quite abruptly, other loop tops begin to appear above them. A similar observation was made by Hinotori on 13 May 1981, when the tops of flare loops stayed at the same altitude for 12 min (Tsuneta et al., 1983). No Hinotori data are available before, or after, this period so that no abrupt jump could be verified; but it is clear from Figure 1 that, quite analogically, 12 min of stationary altitude could have been seen by Hinotori if it had observed the 21 May 1980 flare.

A similar phenomenon, a growth of loops through abrupt jumps, was seen before in some H α movies of post-flare loops. Whereas, however, the jumps seen in H α might have been due to effects of differences in the cooling of plasmas at different initial densities, the X-ray jumps are clearly related to the loops excitation or formation. It is of interest that Forbes and Priest (1983) theoretically predicted the existence of multiple X-type neutral lines at different altitudes above two-ribbon flares, where distended field lines may subsequently reconnect and thus produce new sets of loops at different altitudes.

Figure 2 shows an enlargement of the abrupt rise in altitude that is seen in 21:12 UT in Figure 1. If the loops were radial, the rise would represent a jump from 26 000 to 43 000 km altitude. Figure 2 demonstrates that the rise was first seen in the highest energy channel (22 to 30 keV) with a later follow up at lower energies. This can be interpreted as a new release of energy in a very small volume of plasma at extremely high temperature (Svestka and Poletto, 1985). For an illustration, let us enhance the temperature of a small volume in the corona from 20×10^6 K to 50×10^6 K. Then the X-ray flux from this volume rises by a factor 2200 in the hardest HXIS band 6, but only by a factor of 3 in the softest band 1. Therefore, we can see the source in band 6 in spite of its small dimensions, whereas in lower-energy bands we must wait until its emission measure substantially increases. An obvious candidate for the process we observe here is the reconnection of field lines, in apparent agreement with the Kopp and Pneuman (1976) model of the formation of post-flare loops (in the basic configuration suggested by Sturrock (1968), and with the multiple neutral lines deduced by Forbes and Priest (1983)).

One has to be aware of the fact that the collimating techniques of HXIS may be partly responsible for the observed jumps in altitude: if the loops were thin, we would see them emitting in one HXIS pixel as long as they travel through this pixel, and “jump” in another pixel when leaving it. Broader loops will smear this “pixel-effect.” On the other hand, it is of interest to note that the spatial resolution of Hinotori deteriorates with the growing size of the imaged source: thus moving loops must be quite extensive to be seen by Hinotori at a “constant” altitude for 12 min. Thus moving loops would be seen by HXIS at a fictitiously constant altitude if their real thickness was $\ll 8$ arc s, and by Hinotori if their thickness was $\gg 8$ arc s. This difference in imaging tends to support the supposition that the observed jumps in altitude were real.

In any case, new loops appeared at $\sim 21:12$ UT at a higher altitude and were first seen in the highest energy band of HXIS. A unique set of parameters of the new source of energy release cannot be deduced from the available data. However, a reasonable agreement with the observation is found for a source with temperature of 50×10^6 K between 21:08 through 21:13 UT, growing in size (supposedly as an arcade of loops was formed) and reaching emission measure of $3 \times 10^{45} \text{ cm}^{-3}$ at the end of its development. Then the source cooled, and its emission measure was fast increasing (possibly through evaporation of chromospheric material into the new loops) to $3 \times 10^{47} \text{ cm}^{-3}$ at 21:17 UT, i.e., by two orders of magnitude during 4 min. Table 2 gives the estimated size of the new source of energy release at 21:13 UT for various (unknown) electron densities.

Figure 3 shows images of the flare from 21:09:17 UT onwards, in the six energy bands of HXIS. The image in band 4 at 21:09:17 presents the typical situation seen in all bands at earlier times: a maximum of brightness at a distance $d \cong 9000$ km from the $H_{\parallel} = 0$ line, marked here

approximately by the active region filament. In band 6, at that time, we see already an extension of the flux-contours to the south. This extension is more pronounced at 21:10:38, and finally a new maximum is formed, more to the SW, i.e., at a higher altitude, at 21:12:00 UT (marked by A in Figure 3). This is the site we begin to see at $d \cong 15,000$ km in Figures 1 and 2. At lower energies this new brightening occurs successively later, as we have indicated by arrows in Figure 3.

The new brightening at A occurred 23 min after the flare onset and 17 min after the maximum in the hard X-ray burst. Thus it represents an energy release late in the post-maximum phase of the flare, which gives direct evidence that, in two-ribbon flares, energy is still being released after the impulsive phase is over.

(a) Pixel gain

Figure 3 can also be used for a demonstration of one of HXIS deficiencies: inhomogeneities in the gain of HXIS pixels; the gain G of a pixel is defined as the ratio between the outgoing signal and the energy of an incoming photon.

Most pixels do not deviate by more than 3% from the nominal gain $G = 1.00$. However, there are 20 pixels in the HXIS fields of view (out of 400) for which either $G \geq 1.05$ or $G \leq 0.95$. A difference in gain changes the effective energy band boundaries from E to E/G . How serious this effect can be is apparent from the pixel marked B in Figure 3. With $G = 1.05$ it images in HXIS band 6 X rays between 20.9 Å and 28.6 Å (instead of 22.0 Å and 30.0 Å) and thus creates a fictitious maximum in the brightness contours. As Figure 3 shows, the effect is most serious in the high-energy channels, but it has to be considered at the low energies as well when temperature maps are made (cf. Section III).

III. POST-FLARE ARCHES

The very low background of HXIS made it possible to detect large arch-like structures in the solar corona, which are formed, or become enhanced, after two-ribbon flares. Flares of other kinds do not affect them. These arches are seen in >3.5 keV X-rays for 10 hours or more, and temperature in them may exceed 20×10^6 K. Some appear to be stationary, while others show moving maxima of brightness associated with thermal disturbances propagating upwards with speeds of ~ 10 km/s. It appears that essentially every arch forms the base of a type I radio noise storm which developed from a stationary radio type IV burst initiated by the flare. Machado et al. (1983) imaged a similar structure in 3.5 to 5.5 keV X-rays above a type I noise storm source during its whole transit across the solar disc.

(a) Stationary arch of 21/22 May 1980

Figure 4 shows 3.5 to 5.5 keV images of the coronal arch seen after the two-ribbon flare of 21 May 1980, 20:52 UT (Svestka et al., 1982a; Svestka, 1983). These are half-an-hour integrations of an extremely weak coronal structure: the count rate of the peak in the last image, at 06:36 UT, only slightly exceeds 1 count/min; yet, this is still four-times more than the average background.

One can see that the brightest part (apparently the top) of the arch stayed in the same position since 03:20 UT (6.5 hours after the flare) until the end of the HXIS imaging. Unfortunately, SMM did not look at this active region for two orbits preceding 03:30 UT. Last images

prior to that are from 23:07 UT on 21 May when the post-flare loops still fully dominated the field so that it was extremely difficult to distinguish the much weaker coronal arch. Nevertheless, a careful analysis succeeded to separate the arch from the loops and the results are shown in Figure 5 (Hick and Svestka, 1985): since 23:02 UT the top of the arch was in the same position as in the much later images of Figure 4. Prior to that, from the beginning of the orbit at 22:28 UT, the maximum was in a neighboring pixel, but still at about the same altitude above the flare. If one follows the time development of the X-ray flux in these two pixels (and that is another great advantage of HXIS that it allows such local (8 x 8 arc s) photometry) one finds that the flux in the first pixel peaked at ~22:56 UT, whereas the other pixel peaked some 10 min later and since then stayed to be the brightest pixel in the field (Figure 6).

(1) Spatial resolution

These extensive coronal structures could be seen in the coarse field of view only, because of its lower effective background and much larger covered area on the Sun. For these advantages of the coarse field, however, we pay with very low spatial resolution of 32 arc s (FWHM). It is clear from Figure 4 that very little can be said about the real structure of the detected coronal arch. But sometimes indirect information gives some insight into the unresolved formations, like in Figures 5 and 6; e.g., one can tentatively conclude that the arch consisted of (at least) two separate arch-like structures, since they peaked in brightness at slightly different times.

Another restriction, caused by the low spatial resolution, applies to observations of any motions. A “stationary” source, seen for one hour in the coarse field of view, still could move by up to 0.53 arc s per minute (~6.5 km/s in projection on the disk) without its motion possibly being recognized. In our case, we saw the top of the arch in stationary position for 8 hr 20 min, which allows for a maximum motion of 0.78 km/s in projection. Thus, in this case we may really safely conclude that the arch was a stationary structure.

(2) Flare mode

A great obstacle in the study of these coronal structures near the time of their origin was the flare mode of HXIS operations: as soon as there was a flare (or the X-ray flux exceeding a certain limit), HXIS changed its normal observing interval of 7.5 s to 1.5 s and compensated for the lost time by omitting the imaging of weaker pixels. The aim of this special mode was to enhance the time resolution during flares and, of course, the main part of the flare was always imaged. However, any weaker features, including the coronal arches and potential X-ray counterparts of flare-associated radio bursts, disappeared from the images. This contributed to our difficulty to obtain the arch images in Figure 5 (when HXIS was in flare-mode 2 with time resolution of 4.5 s) and made it completely impossible to see anything from the arch in the orbit before, when the flare began (when HXIS was in flare-mode 1, with time resolution of 1.5 s). It is very regrettable that HXIS was suppressing data since we are unable to get any information whatever about the origin of this kind of post-flare coronal structures.

(b) Reviving arches of 6/7 November 1980

Another example of a post-flare coronal arch was recorded on 6 November 1980, after a major two-ribbon flare at 03:04 UT (imp. X9), which had not been seen by the SMM, but the spacecraft pointed to the flaring active region since 06:20 UT. This arch (or post-flare coronal cloud, since we have no direct evidence in this case, projected over the solar limb, that it was an arch structure) had many features common with the event of 21/22 May (Svestka et al., 1982b).

However, there was a very significant difference: the maximum of brightness was not in a stationary position, like in 21/22 May, but it was rising in the corona, as Figure 7 clearly demonstrates. Before this arch completely disappeared, it was revived, at 14:40 UT, after the occurrence of another two-ribbon flare in the same active region, and we saw again the same rise of the maxima in brightness as at the flare before (Figure 7). The two events were quite homologous (Svestka, 1984b).

This rise of a coronal disturbance after the flare can also be demonstrated in another way. Figure 8 shows a series of temperature maps, constructed from the flux ratio of HXIS bands 1 and 2, in the fine field of view of HXIS (Svestka, 1984a). One can see that shortly after the flare (the upper times in each frame) an extended region of high temperature was formed (with $T > 20 \times 10^6 \text{K}$) which moved upwards across the solar limb and eventually disappeared from the fine field of view of HXIS some 2 hr 15 min after the flare. The continuation of this rise, in brightness of the arch, can then be further followed in the coarse field, as shown in Figure 7.

The arch revived once again at $\sim 04:40$ on 7 November, and it is very likely that already the first appearance of the arch (the upper row in Figure 7) was a revival, since a major two-ribbon flare at 13:41 UT on 5 November (not seen by the SMM) was probably the source of the first arch formation. Our present interpretation is (cf. Svestka et al., 1982a) that the post-flare arch is the upper product of the reconnection process which forms the post-flare loops below. The first arch is formed fast near the onset of the flare (Hick and Svestka, 1985) and the maximum stays in a constant position since its formation. When an arch revives, however, the new arch meets an obstacle at its formation – the pre-existing arch – and this leads to the gradual rise of the arch excitation seen in Figures 7 and 8 (Svestka, 1984b).

We have studied in detail the second arch on 6 November (following the flare at 14.40 UT), since this is the only arch we could observe during its whole development. Figure 9 shows the results: the arch began to brighten, and its temperature began to rise, from the very onset of the two-ribbon flare. The temperature reached its maximum about 1 hr later, the brightness in 3.5 to 5.5 keV X-rays peaked about 2.3 hr, and the emission measures more than 3 hr after the flare onset. It looks like a flare, with both the size- and time-scale enlarged by an order of magnitude. The physical characteristics deduced for this revived arch are summarized in Table III. One can see that the energy contents and mass are comparable to an average coronal transient (cf. the paper by N. R. Sheeley in these proceedings).

(1) Temperature measurements

When determining temperature from HXIS data (Mewe et al., 1985), we have encountered serious difficulties in the calibration of the energy band 2 which contains the helium-like complex of iron (Svestka and Poletto, 1985). As soon as temperature exceeds $20 \times 10^6 \text{K}$ (or during the impulsive phase, whichever statement is correct), the emission in band 2 is clearly overestimated, since $T(2/1)$ results higher than $T(3/2)$. The reason for this may be an incomplete knowledge of satellite iron lines which begin to become important for $T > 20 \times 10^6 \text{K}$, or perhaps an excitation by particle streams, whereas the calibration assumes Maxwellian distribution of velocities. In any case, one should avoid band 2 in temperature measurements if T exceeds $20 \times 10^6 \text{K}$. That is the reason, for example, why we have determined T from the bands 1 and 3 and not 1 and 2 (with better statistics) in Figure 1.

(2) Temperature maps

This uncertainty in the calibration of HXIS band 2 does not have much influence on the studies of coronal arches, since temperature in them is generally lower. However, other disturbing effects appear when constructing the temperature maps of the corona, and one has to be particularly cautious when preparing them.

First, there are ghost images produced by the collimator which appear towards the NS and WE directions from a bright source. They are extremely weak and usually do not play any disturbing role in the X-ray images. However, the ghosts are more intense at high energies; since temperature is determined from the flux ratios, irrespective of the flux intensity involved (provided there are enough counts to make the ratio statistically significant), these ghosts clearly appear as fictitious maxima in the temperature maps.

This effect of ghosts had been known before the launch and can be corrected if necessary. However, there is another effect which had not been expected, and which puzzled us for quite some time: if there is a bright flare source, we can see not only the ghosts in the temperature maps, but also temperature maxima elsewhere around the flare, sometimes producing almost a circle, or a semi-circle with the flare close to its center. First we thought, and Harrison and Simnett (1985) still believe that it is at least partly true, that we saw here the X-ray light from the source backscattered on the photosphere. However, Fárnik (private communication) has found cases when such temperature maxima were seen also above the limb. Therefore, we are now convinced that the effect is mostly, and possibly completely, due to an instrumental effect: the FWHM of the HXIS pixels increases with increasing energy. Thus wherever the gradient of X-ray flux is high (like at a certain distance around the flare), the outlying pixels have a larger contribution from the high energy bands, which leads to a fictitious enhancement of temperature along the high-gradient boundary around the flare. A weak example of it can be seen in the first image in Figure 8, at 3 min 46 s before the peak of the impulsive phase of the flare (compare it with the flare position in the lower central frame of Figure 8). The effect is slightly visible in the other upper-row maps as well.

Therefore, we must always carefully check whether there is any instrumental effect (ghost, high gradients of flux) potentially responsible for maxima detected in temperature maps. Note that the accumulated isophotes at the left-hand side of the upper images in Figure 8 do not mean a high gradient of flux; they only mark the boundary where the flux ratio exceeds the statistical significance of 3σ . So the maxima in Figure 8 are real temperature enhancements traveling across the limb.

Also the inhomogeneous gain of HXIS pixels (cf. Section II) can produce false maxima in temperature maps similar to that one in flux demonstrated in Figure 3, even at lower energies (Svestka and Hick, 1985). Since, however, the gain for different pixels is known, this effect can be easily recognized and to a great extent eliminated.

IV. INTERCONNECTING LOOPS

After the discovery of the reviving postflare arches on 6 November 1980, Fárnik et al. (1985) became interested in the further behaviour of this active region which was followed by the SMM up to its disappearance behind the western limb on 20 November. First they found another revival of the arch, late on 7 November and on 8 November (Figure 10), but the situation completely changed on 9 November. On that day another coronal structure appeared (Figure 10,

right-hand picture) which extended towards the SE, instead of SW. Since this structure first appeared after a major flare in another active region 17 251 (cf. Figure 10), Fárnik et al. have assumed that HXIS imaged here a big loop interconnecting the observed region 17 255 with the (invisible for HXIS) region 17 251.

The two structures shown in Figure 10 definitely differ in their nature. The arch (to the SW) always revived after a two-ribbon flare in the region below it. The structure towards the SE behaved in relation to flares in a way very similar to that found for interconnecting loops during Skylab (Svestka and Howard, 1979): some flares (in both active regions) seem to enhance it; these definitely need not be two-ribbon flares; other flares have no impact upon the structure, and sometimes the structure brightens without any obvious flare association.

A very similar coronal structure, with the same loose association with flares, was also detected by Harrison et al. (1984) on 29 June 1980. Images of this interconnecting loop on the limb are shown in Figure 11 (left). The interconnecting loops could not be seen on the disk, but simultaneous X-ray brightenings in both the regions, like in the right-hand image of Figure 11, on 24 June, had suggested the existence of a coronal interconnection already on that day (Simnett et al., 1984).

Another difference between the SW arch and the SE structure in Figure 10 was the cooling time of the X-ray brightenings. The life time of the enhancements of the SW arch was 14 hr or more, whereas all enhancements of the SE structure were relatively short-lived; the SW arch shown in Figure 7 cooled for ~ 6 hr from $T = 14 \times 10^6$ K to $T = 8 \times 10^6$ K, whereas in the strongest brightening of the SW structure on 11 November the same temperature decrease was accomplished within 80 minutes. With the densities deduced (of the order of 10^9 cm $^{-3}$) this indicates that the heat conduction was inhibited in the SW arches, but active in the SE structure. This is to be expected with the complex magnetic structure of the arch, originating through a long-lasting sequence of reconnections and possibly even detached from the surface, in comparison to a simple-structured loop that interconnected two active regions.

(a) The field of view

Though there are strong arguments supporting the suggestion that the structure seen on 9 November and later on was an interconnecting loop, one can never be sure of it, since the other interconnected region was out of the field of view. This is only one demonstration of the disadvantages of the restricted field of view used by HXIS and other SMM instruments. In Figure 1 we could not study the thermal wave (analogic to Figure 8), because it was out of the fine field of view. The western footpoint of the arch of 21/22 May 1980 was out of the coarse field of view (Figure 4). The thermal wave disappeared from the fine field of view in Figure 8 and both the arches in the morning and afternoon of 6 November extended out of the coarse field of view (Figure 7). Besides, lots of interesting events (e.g., all γ -ray flares) were missed by the SMM and HXIS in 1980, because the spacecraft was pointed to another region on the Sun.

V. PRE-FLARE ENHANCEMENTS

Another unexpected discovery made by HXIS were X rays emitted by hot plasma in absence of flares. Schadee et al. (1983) have found that some active regions are characterized by long-lived X-ray enhancements above 3.5 keV along the filament channels. These sources are $\sim 10^4$ times weaker than a flare, can last for several hours, and some possibly mark the sites

where a major flare will occur many hours later. The temperature deduced for them from the HXIS bands 1 and 2 exceeds 10×10^6 K.

The low resolving power of the coarse field of view of HXIS makes it impossible to decide whether there is really an exact coincidence in position between these pre-flare enhancements and the coming flare. Only in the "Queens' " limb flare of 30 April, 1980 (De Jager et al., 1983), these pre-flare enhancements could also be seen in the fine field of view; most of them were then not in exact coincidence with the position of the flare; however, for 26 min prior to the flare an enhancement, faint but distinct, coincided exactly (within the resolution of 8 arc s) with the flare position. Also its shape was similar to the shape of the coming flare event.

Other active regions show a high number of short-lived X-ray variations, about 10^{-3} times weaker than a flare, which probably are X-ray mini-flares. Galzauskas, Schadee and Martin (private communication) succeeded to associate a few of them with tiny H α brightenings.

An extremely interesting observation has been reported by Simnett and Harrison (1984) and Harrison et al. (1985): They claim that at a time consistent with a coronal mass ejection onset at the very early phase of a flare there is a small, soft X-ray burst (a precursor) which may signify the origin of the coronal transient. Figure 12 shows an example of such an event. The images of the preflare brightening at times marked a, b, c in Figure 12 are shown in Figure 13. The preflare structure really seems to rise near the time when an accelerating mass ejection might have started.

VI. CONCLUSIONS

We have tried to demonstrate that the hard X-ray imaging can yield data on many more coronal phenomena than just the impulsive (hard X-ray burst) phase of flares. There are X-ray enhancements in non-flaring active regions corresponding to mini-flares, long-lived high-temperature disturbances along filament channels, and flare precursors. Some of them may signify the origin of mass ejections prior to flares. Others perhaps indicate the site where the coming flare may occur. After the impulsive phase of a flare, X-ray images show post-flare loops in the shape close to their formation and may reveal new sites of field-line reconnections. After two-ribbon flares, giant post-flare coronal arches are imaged in X-rays, and their energy contents are comparable to the energy contents of coronal transients. They appear to be an important component of the post-flare corona and represent X-ray counterparts of stationary type IV bursts and type I noise storms. Also a few loops interconnecting active regions could be imaged by HXIS.

In the future hard X-ray experiments one should try to image the whole Sun (or at least, large fields of view on the Sun), since the limited fields of view used onboard the SMM caused lots of problems in the evaluation of the data, and many important data were missed. One should not omit lower energies (~ 3 keV), since some important coronal features seem to be prominent at these wavelengths. High spatial resolution is essential, as one can see from many illustrations in this contribution. High time resolution did not prove to be of real significance for HXIS, but this will surely change if, at the same time, also the spatial resolution greatly improves. Nevertheless, the HXIS experience speaks strongly against the use of any suppression of data (flare modes): the gain of this suppression (of which the author admits to be one of the initiators) was essentially nil whereas the losses (no images of type IV, type II, type V radio bursts, no knowledge about the early phase of the post-flare coronal arches) had been very harmful.

In summary, HXIS has been an extremely successful experiment. Its unbelievably low background permitted many new discoveries which had not been expected before the launch. The used techniques had some deficiencies, but these actually became important only at the occasions when we tried to evaluate data very close to the extreme limits of HXIS sensitivity. The present review has tried to summarize all the known pros and contras of the used collimating techniques, for the benefit of those who plan hard X-ray imaging experiments for the future.

REFERENCES

- De Jager, C., 1985, *Solar Phys.*, 96, 143.
- De Jager, C., Machado, M. E., Schadee, A., Strong, K. T., Svestka, Z., Woodgate, B. E., and Van Tend, W., 1983, *Solar Phys.*, 84, 205.
- Fárník, F., Van Beek, H. F., and Svestka, Z., 1985, *Solar Phys.*, submitted.
- Forbes, T. G. and Priest, E. R., 1983, *Solar Phys.*, 84, 169.
- Harrison, R. A. and Simnett, G. M., 1985, *Solar Phys.*, submitted.
- Harrison, R. A., Simnett, G. M., Hoyng, P., Lafleur, H., and Van Beek, H. F., 1984, Proc. SCOSTEP-STIP Symp. on Interplanetary Intervals, p. 287.
- Harrison, R. A., Wagget, P. W., Bentley, R. D., Phillips, K. J. H., Bruner, M., Dryer, M., and Simnett, G. M., 1985, *Solar Phys.*, 97, 387.
- Hick, P. and Svestka, Z., 1985, *Solar Phys.*, submitted.
- Hoyng, P., and 11 co-authors, 1981, *Astrophys. J. (Letters)*, 246, L155.
- Kopp, R. A. and Pneuman, G. W., 1976, *Solar Phys.*, 50, 85.
- Machado, M. E., Somov, B. V., Rovira, M. G., and De Jager, C., 1983, *Solar Phys.*, 85, 157.
- Mewe, R., Gronenschild, E. H. B. M., and Van Den Oord, G. H. J., 1985, *Astron. Astrophys. Suppl.*, in press.
- Schadee, A., De Jager, C., and Svestka, Z., 1983, *Solar Phys.*, 89, 287.
- Simnett, G. M. and Harrison, R. A., 1984, *Adv. Space Res.*, 4, No. 7, 279.
- Simnett, G. M., Harrison, R. A., Hoyng, P., and Van Beek, H. F., 1984, Proc. SCOSTEP-STIP Symp. on Interplanetary Intervals, p. 273.
- Sturrock, P. A., 1968, IAU Symp. 35, 471.
- Svestka, Z., 1983, *Space Sci. Rev.*, 35, 259.
- Svestka, Z., 1984a, *Adv. Space Res.*, 4, No. 7, 179.
- Svestka, Z., 1984b, *Solar Phys.*, 94, 171.
- Svestka, Z. and Hick, P., 1985, *Solar Phys.*, to be submitted.
- Svestka, Z. and Howard, R., 1979, *Solar Phys.*, 63, 297.
- Svestka, Z. and Poletto, G., 1985, *Solar Phys.*, 97, 113.
- Svestka, Z., and 14 co-authors, 1982a, *Solar Phys.*, 75, 305.
- Svestka, Z., Dennis, B. R., Pick, M., Raoult, A., Rapley, R. T., and Woodgate, B. E., 1982b, *Solar Phys.*, 80, 143.
- Svestka, Z., and 8 co-authors, 1983, *Solar Phys.*, 85, 313.
- Tsuneta, S., and 7 co-authors, 1983, *Solar Phys.*, 86, 313.
- Van Beek, H. F., Hoyng, P., Lafleur, H., and Simnett, G., 1980, *Solar Phys.*, 65, 39.

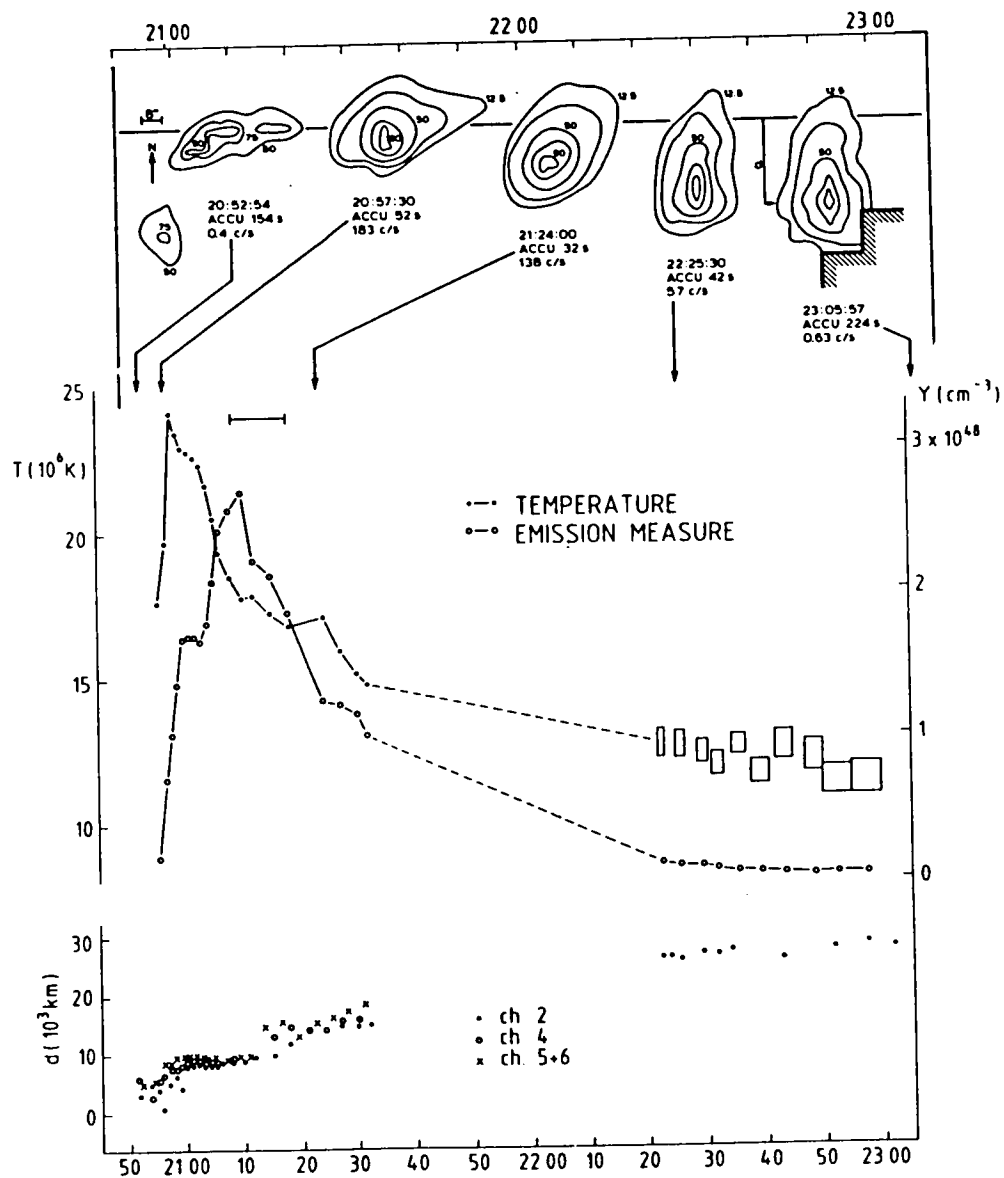


Figure 1. Top: Images of the flare of 21 May 1980 in 3.5 to 8.0 keV X rays. Center: Temperature and emission measure determined from the ratio of HXIS bands 3 and 1, for the four brightest pictures in band 1. (Emission measure Y pixel of fine field of view.) Bottom: The distance of the brightest part of the flare (tops of the loops) from the $H_{\parallel} = 0$ line, d , in projection on the disk, as determined from HXIS bands, 2, 4, and 5 + 6.

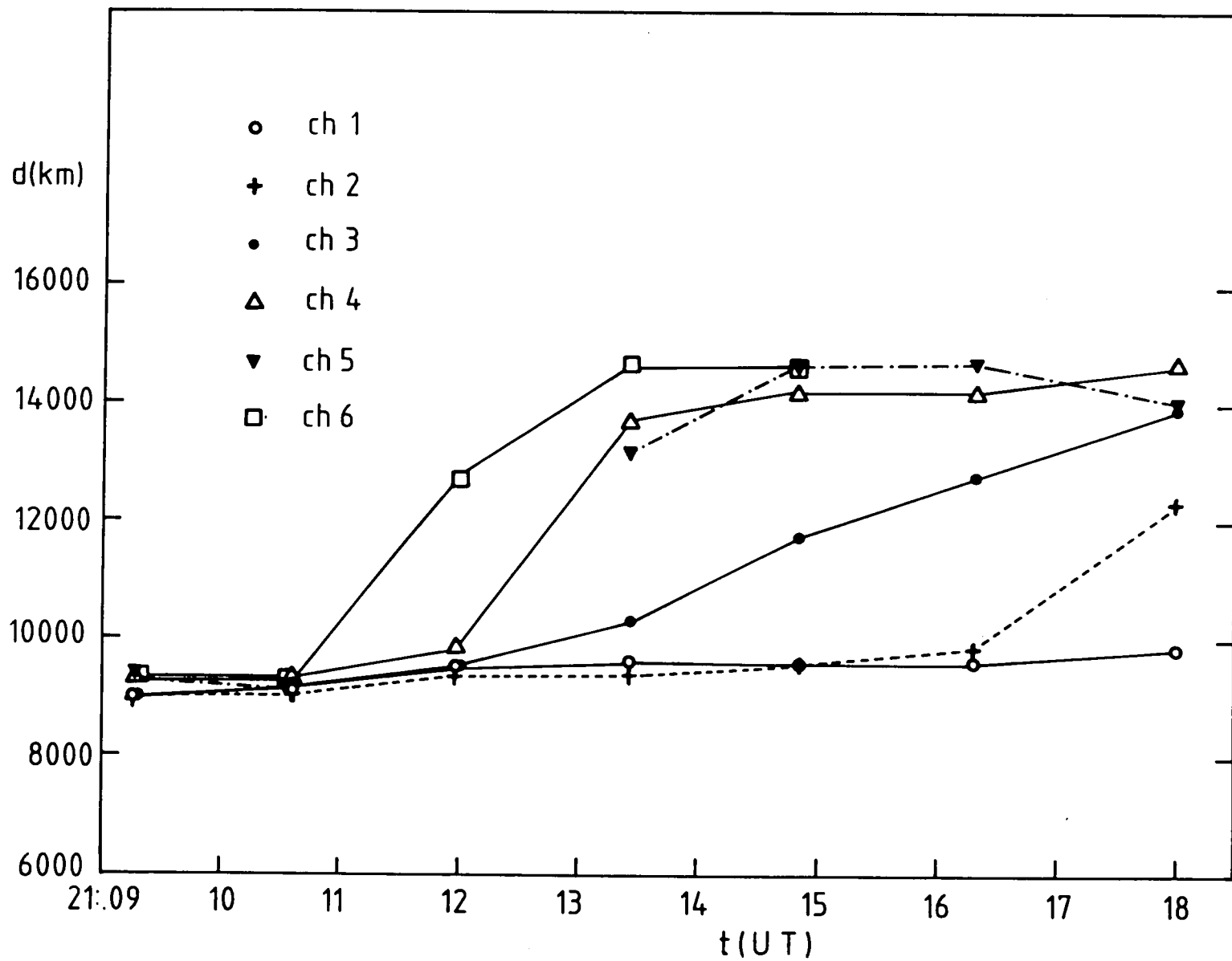


Figure 2. A detail of the variation of d in HXIS channels 1 to 6 during the jump in altitude which occurred at 21:12 UT (cf. the bottom part of Figure 1).

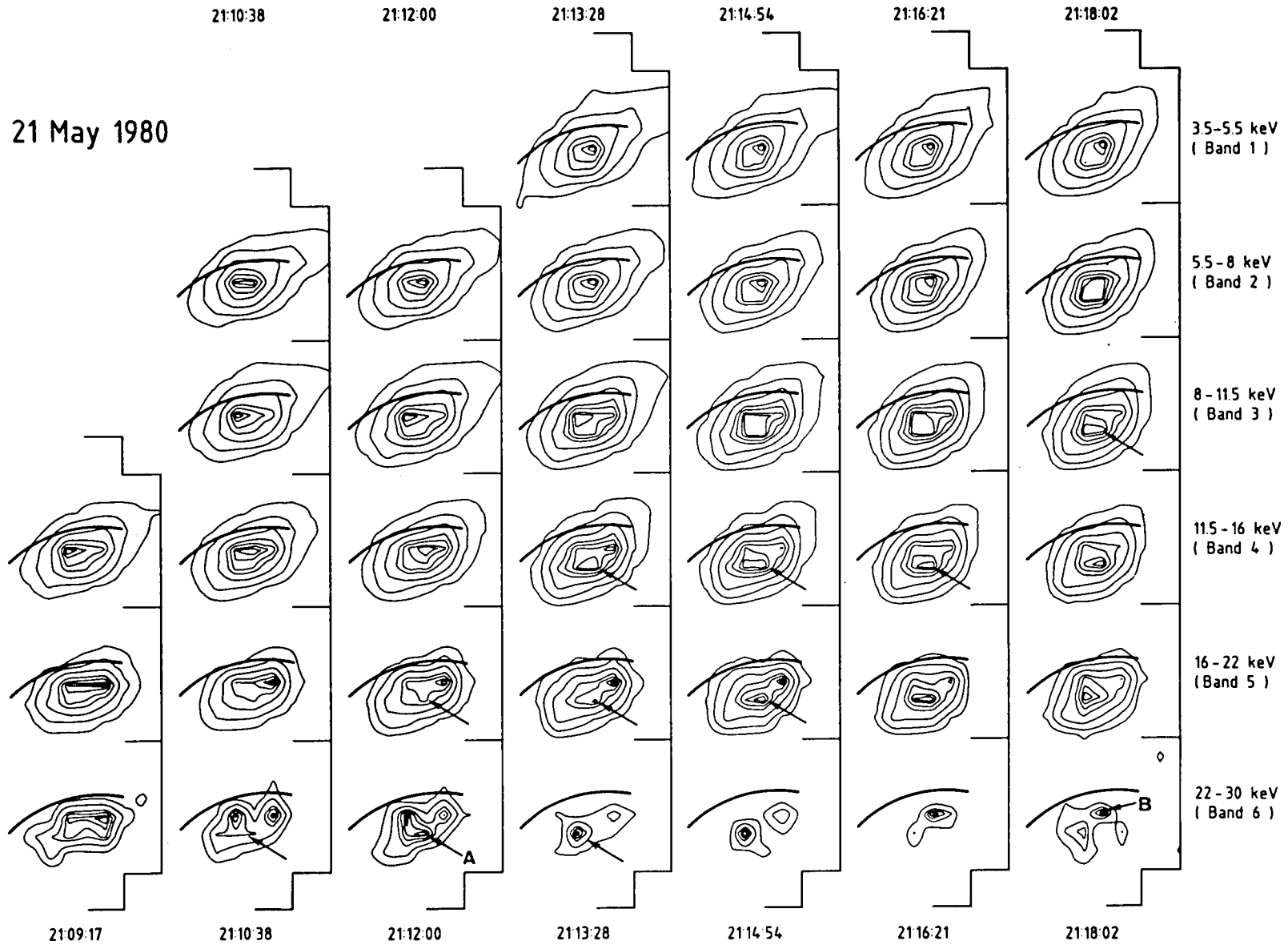


Figure 3. Images of the flare of 21 May 1980 in HXIS bands 1 to 6 during the period from 21:09 through 21:18 UT. The $H_{\parallel} = 0$ line is marked in all the images. North is up, west is to the right. Feature A is a real new maximum; feature B is an artifact (cf. Section II).

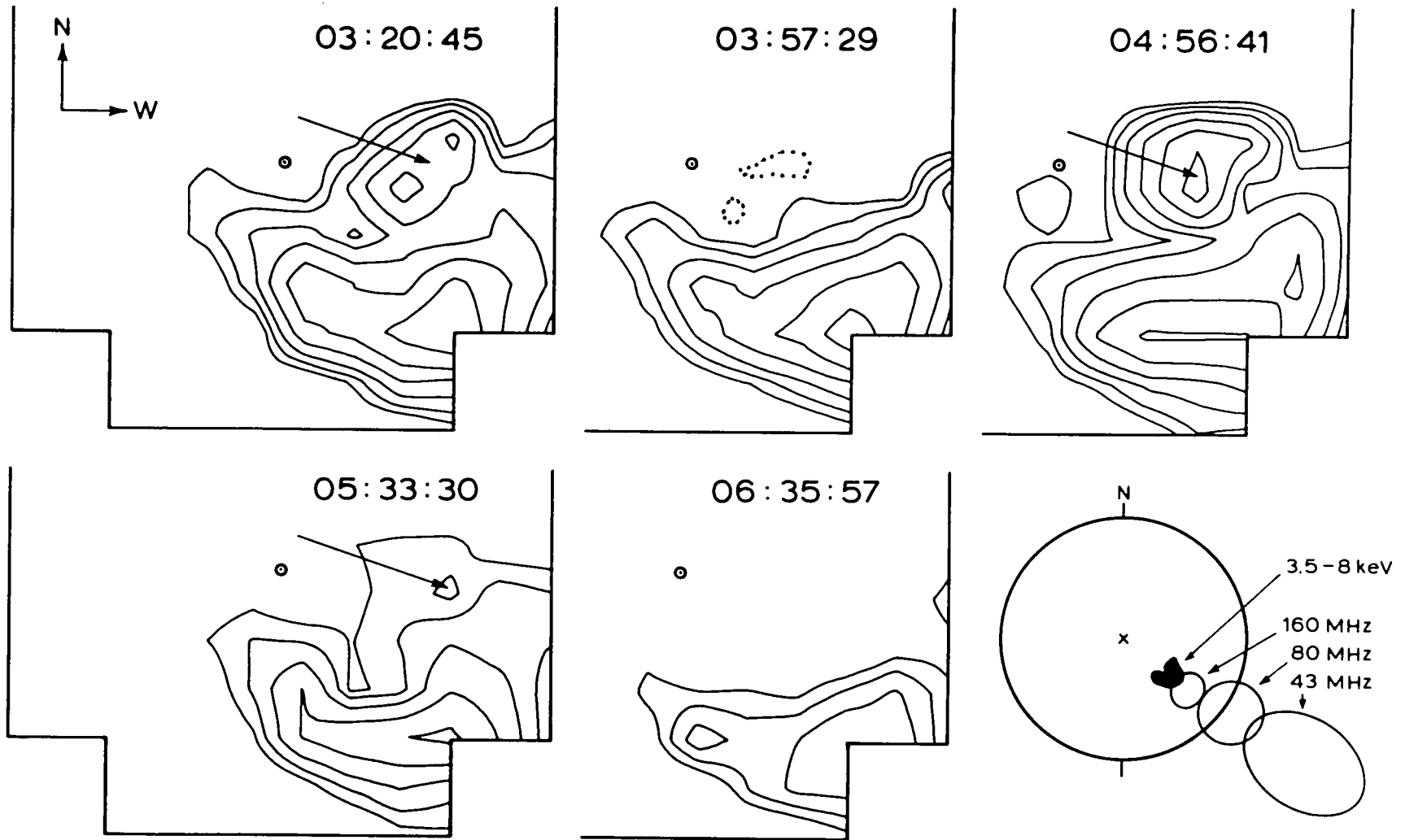


Figure 4. X-ray contours of integrated images of the post-flare coronal arch observed on 22 May 1980. Energy range: 3.5 to 5.5 keV. HXIS coarse field of view, resolution 32 arc s. The given times are mean times of 1525 s integrations. The position of the parent flare at 20:52 UT on 21 May is marked by dotted contours in the upper central image. The insert shows the relative position of the X-ray arch and three radio images of the stationary type I noise storm as seen at Culgoora at 03:20 UT on 22 May.

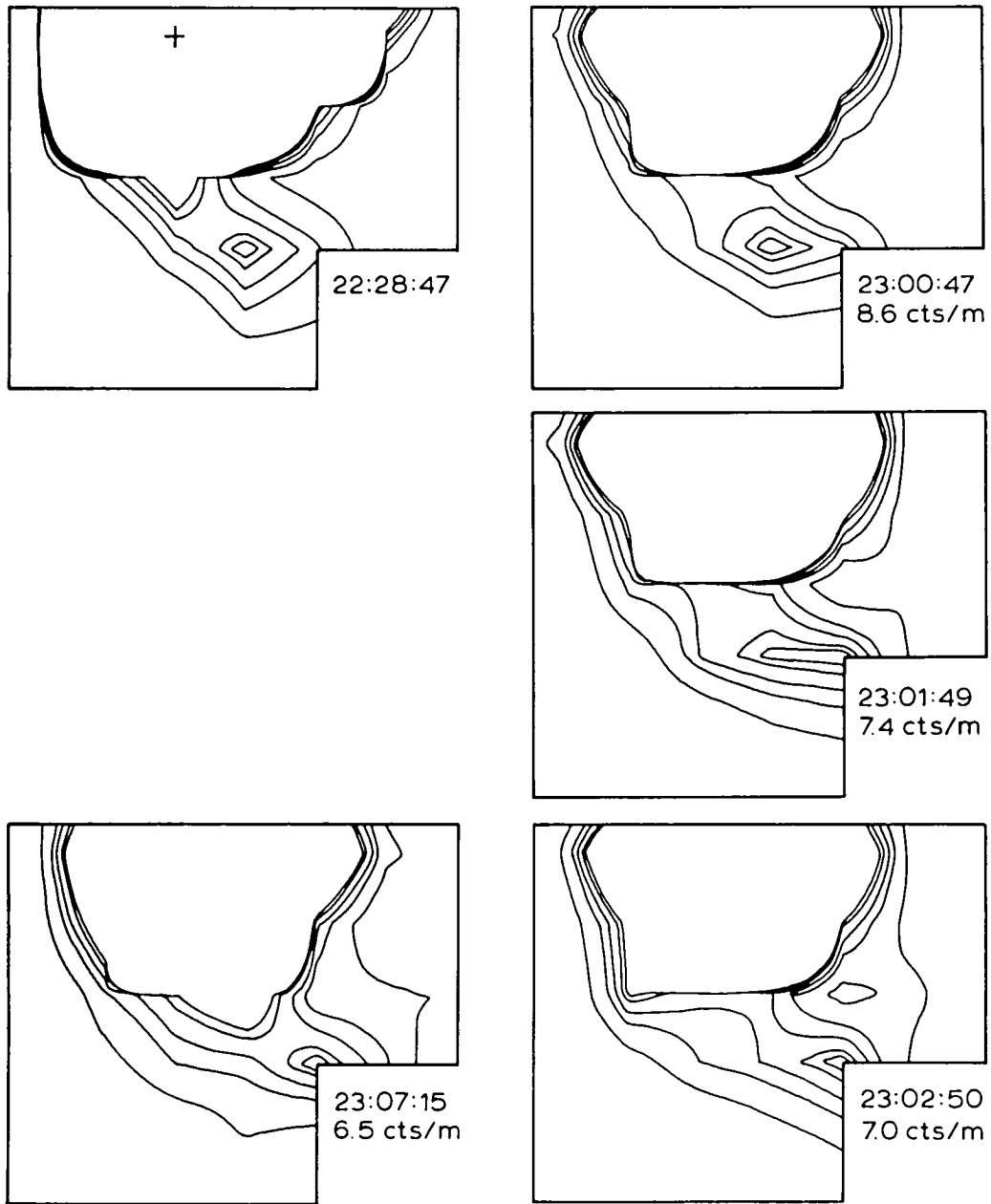
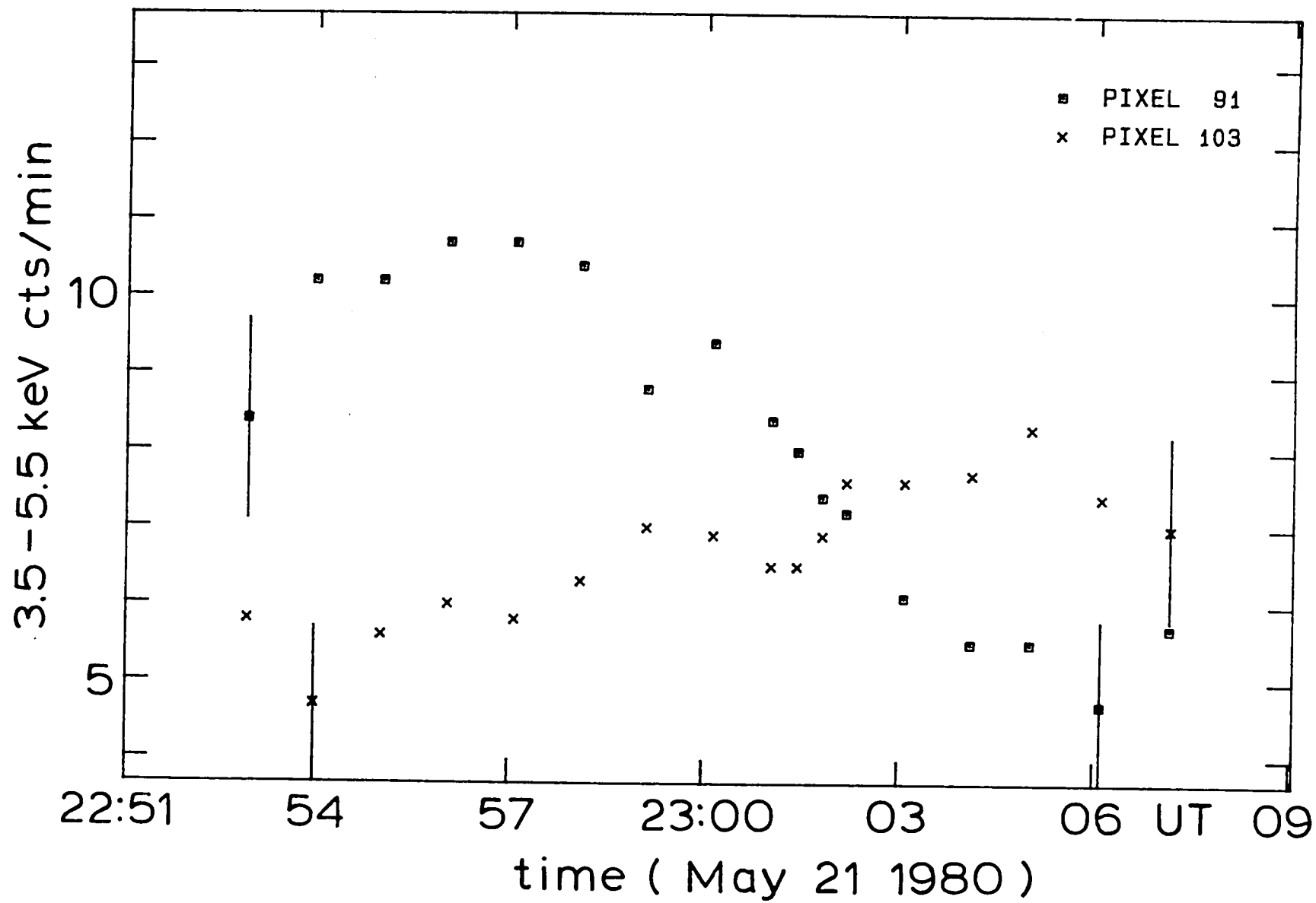


Figure 5. X-ray contours in the SMM orbit next to the flare occurrence at 20:52 UT on 21 May. HXIS coarse field of view, energy band 3.5 to 5.5 keV. The upper and lower images at the left-hand side were recorded at respectively the beginning and end of the SMM orbit. The other three images show the shift of the maximum of brightness in the arch from pixel 91 to pixel 103 at 23:02 UT.



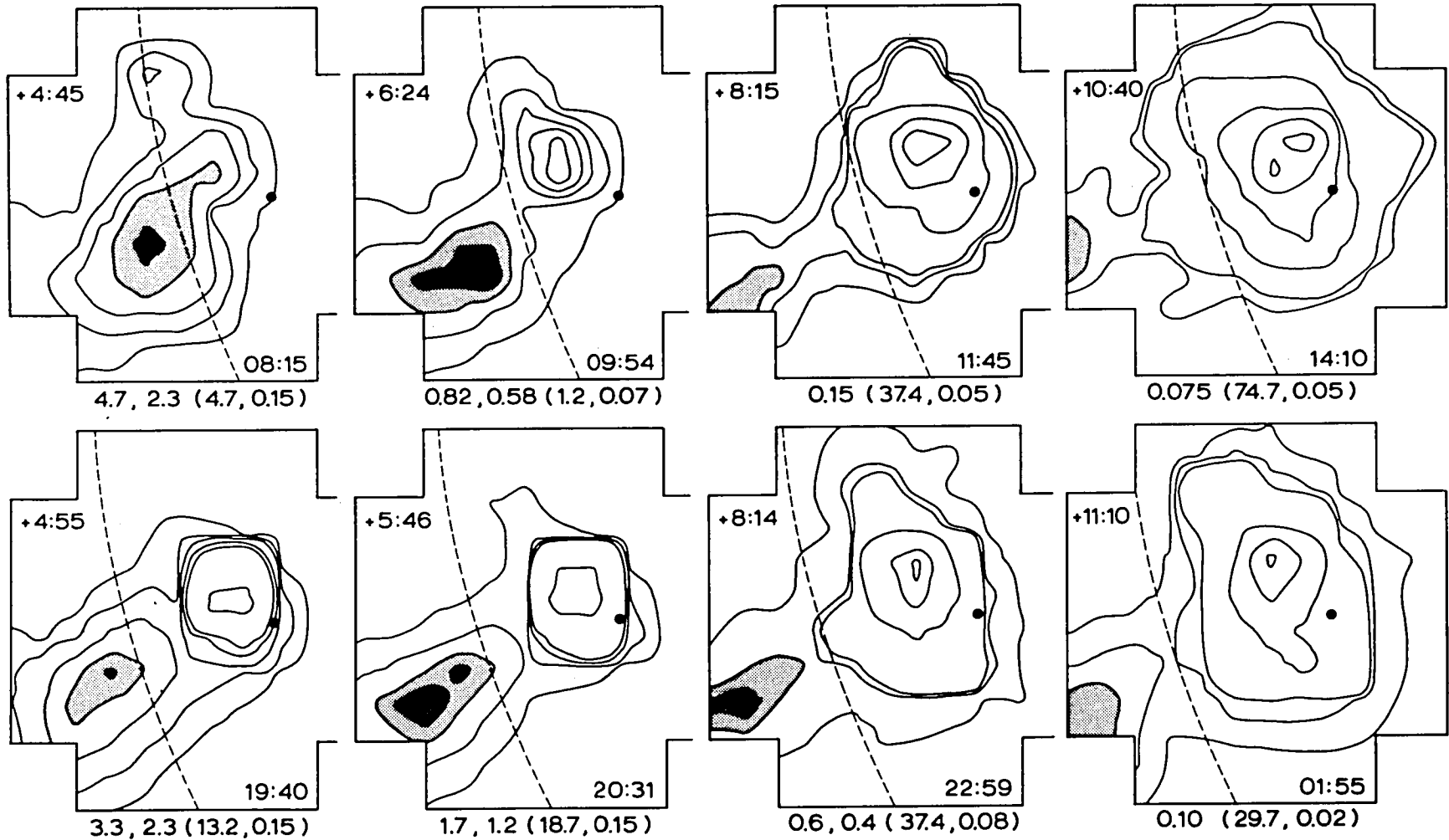


Figure 7. 3.5 to 5.5 keV images of the first and second arch on 6 November 1980 in the coarse field of view of HXIS. The dashed line is the solar limb. In each image the lower-right number is the time of imaging, while the upper-left number is the time elapsed from the onset of the parent flares (respectively at 03.30 and 14:45 UT on 6 November). Numbers below each image give counts/s for the hatched contours in the arch and (in brackets) counts/s for the brightest and least intense contour in each image.

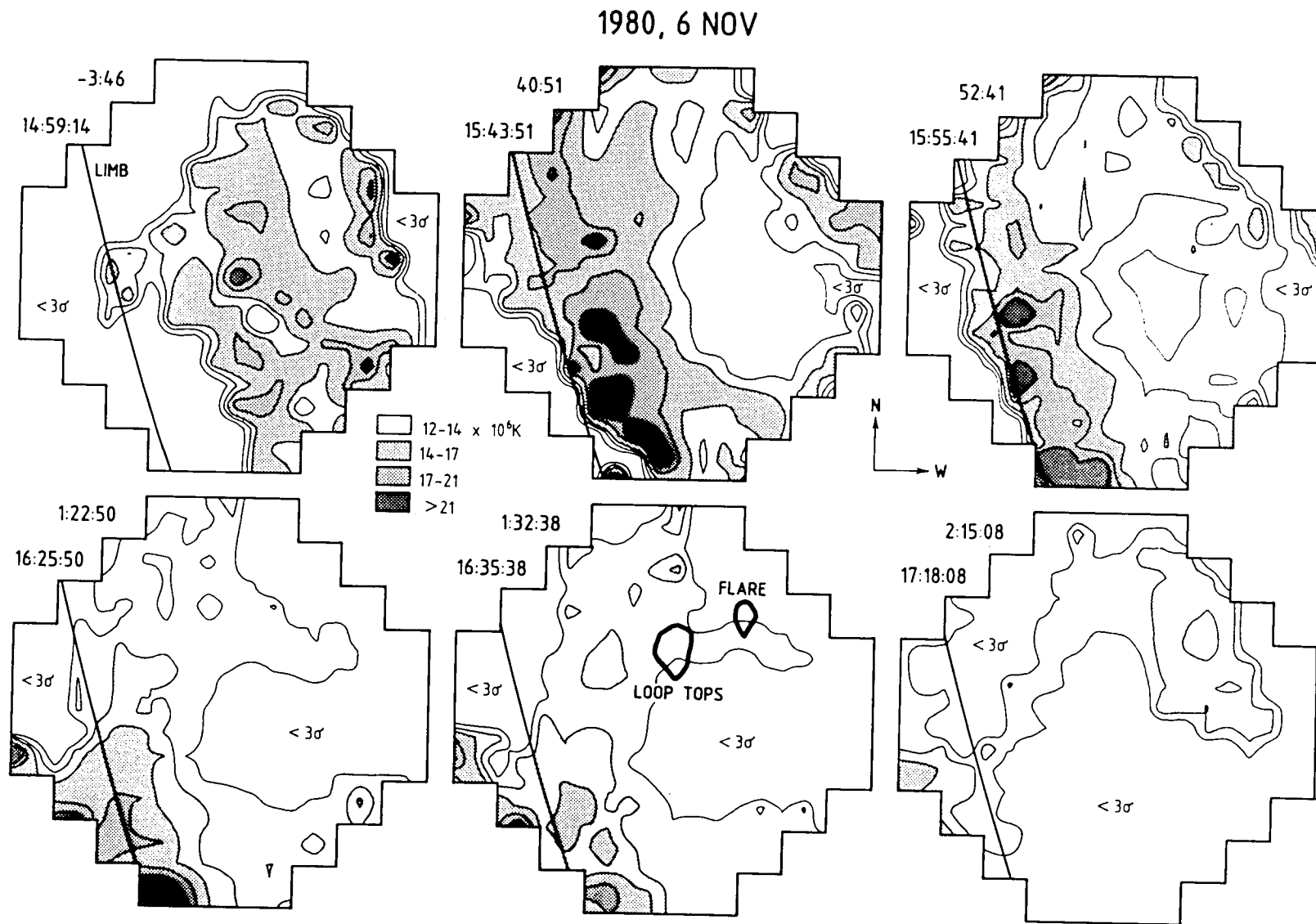


Figure 8. Temperature maps of the early phase of the arch imaged in the lower part of Figure 7. HXIS fine field of view (8 arc s resolution). The contours correspond to 10, 12, 14, 17 and 21 $\times 10^6$ K, as determined from the ratio of counts in HXIS bands 2 (5.5 to 8.0 keV) and 1 (3.5 to 5.5 keV). Only ratios with $>3\sigma$ statistical significance have been used for these plots. Time data give the UT (below) and time difference from the maximum of the flare impulsive phase (above).

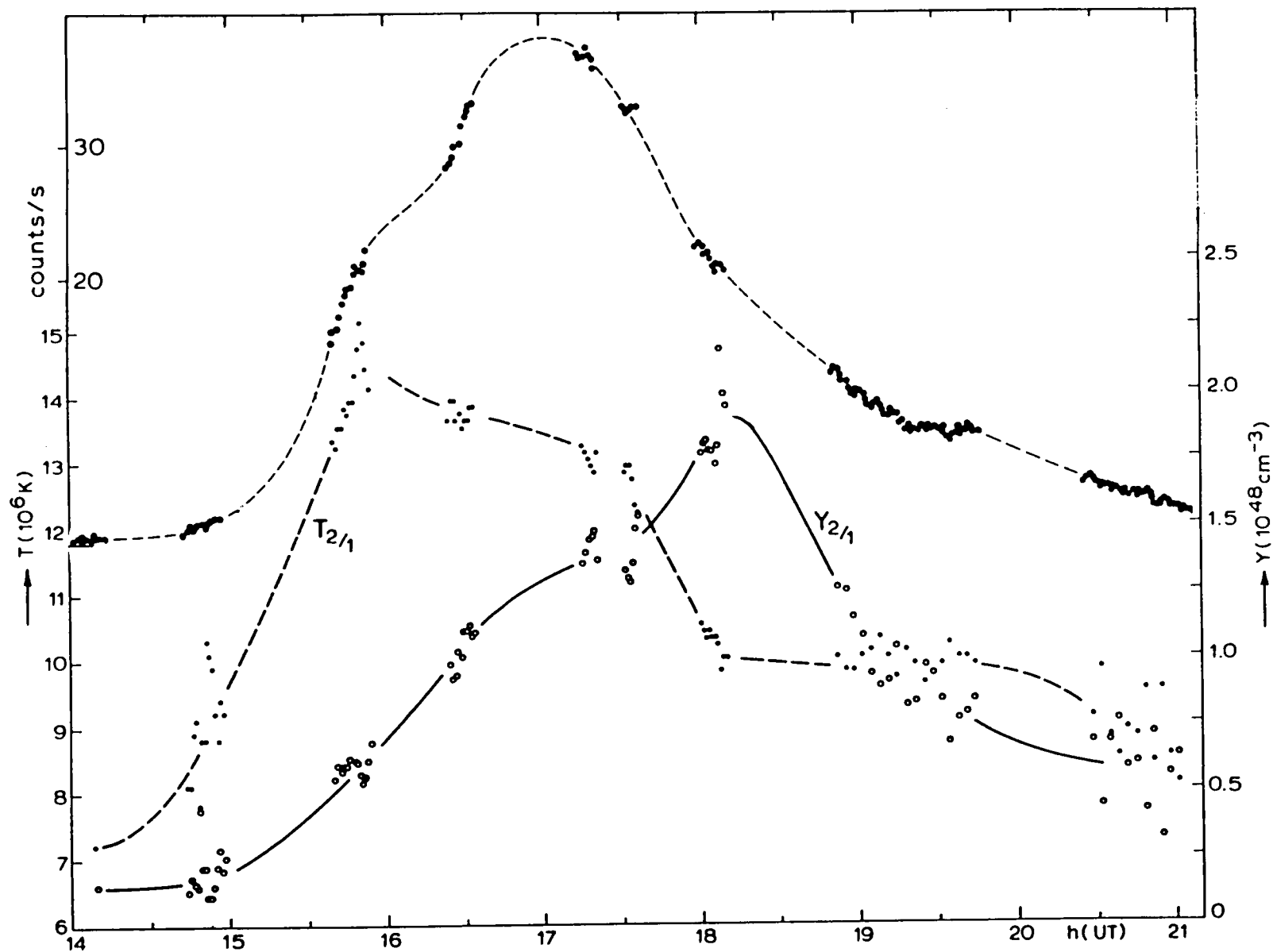


Figure 9. Time development of the arch brightening shown in the lower part of Figure 7. Above: counts/s in 3.5 to 5.5 keV X rays. Below: temperature, $T_{2/1}$, and emission measure per pixel, $Y_{2/1}$, from the ratio of counts in HXIS bands 1 and 2 (5.5 to 8.0 keV / 3.5 to 5.5 keV). These are mean characteristics of 6 pixels of HXIS coarse field of view at an average altitude of 100 000 km.

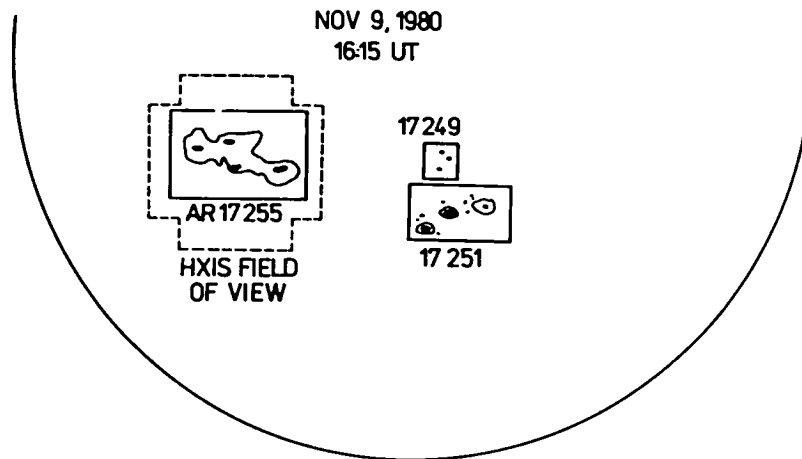
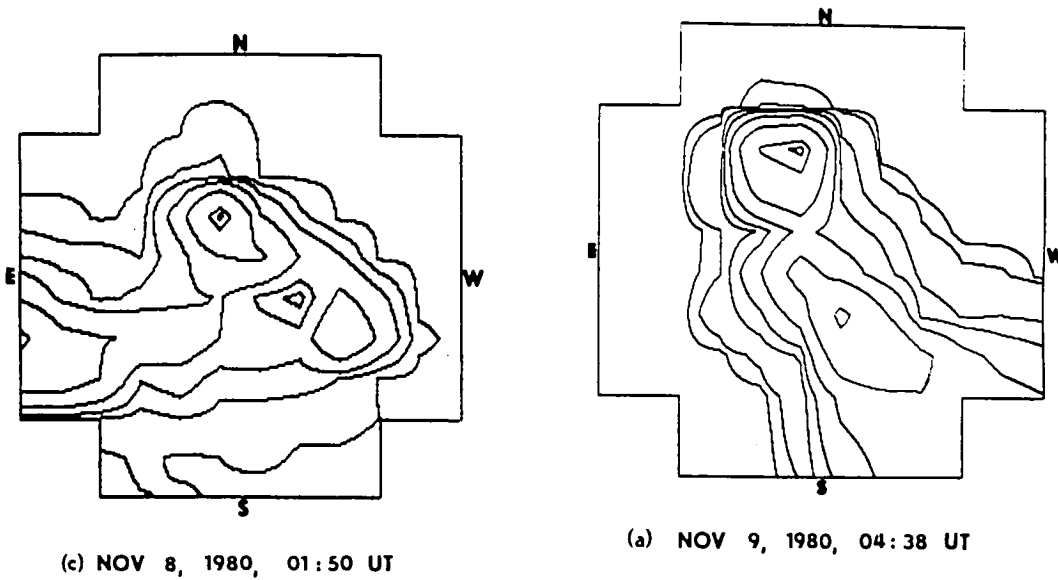


Figure 10. Top: 3.5 to 5.5 keV contours in the coarse field of view of HXIS. Left: the last (probably fifth) revival of the arch shown in Figure 7, on 8 November, 01:50 UT (1008 s integration, maximum count rate 0.7 counts/s). Right: a new structure seen on 9 November, at 04:38 UT (383 s integration, maximum count rate 7.1 counts/s). This new structure may be a loop interconnecting active regions 17255 and 17251, the position of which on the solar disk is shown below.

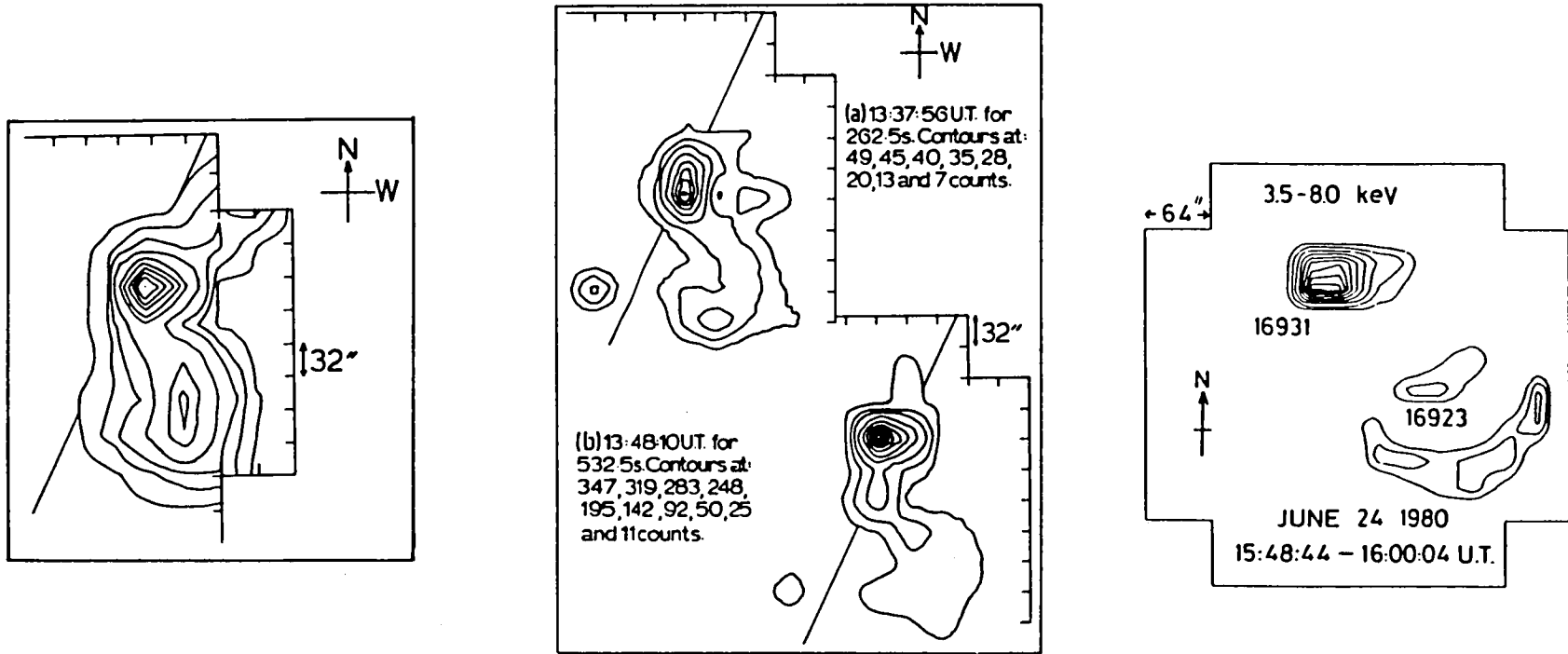


Figure 11. Left: Two X-ray contour plots (3.5 to 5.5 keV) showing the largest of the coronal loops interconnecting AR 16931 and AR 16923 on the western solar limb on 29 June 1980. Right: Five days earlier, on 24 June, simultaneous X-ray brightenings were seen in both these (supposedly interconnected) regions.

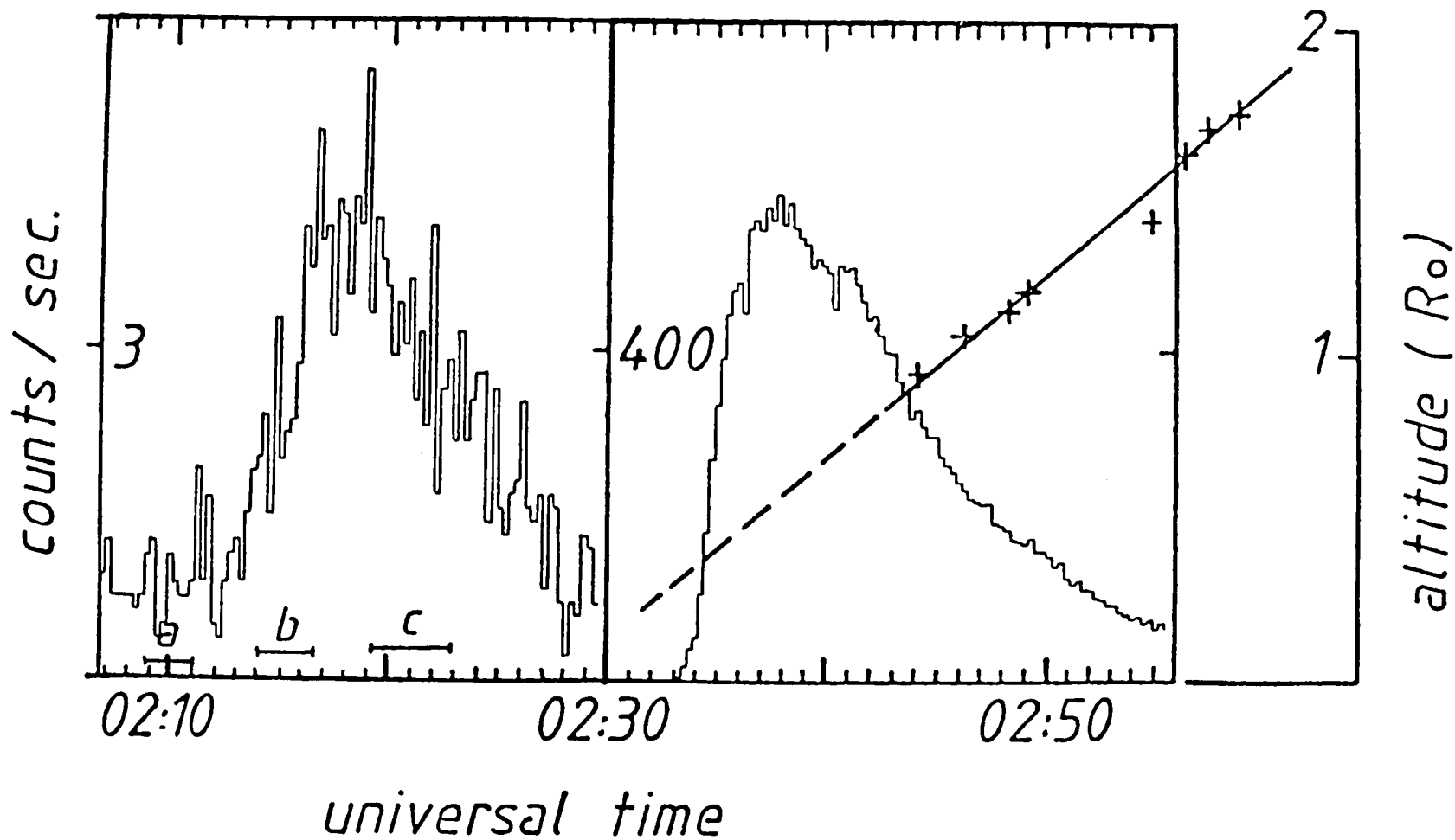


Figure 12. 3.5 to 5.5 keV intensity time profile for the flare at 02:33 UT on 29 June 1980, and its precursor (note the scale change at 02:30 UT). Superposed onto this are the altitude histories of the white-light coronal mass ejection (crosses) and an X-ray transient (a, b, c) which is shown in Figure 13.

SMM-HXIS JUNE 29, 1980 3.5-5.5 keV

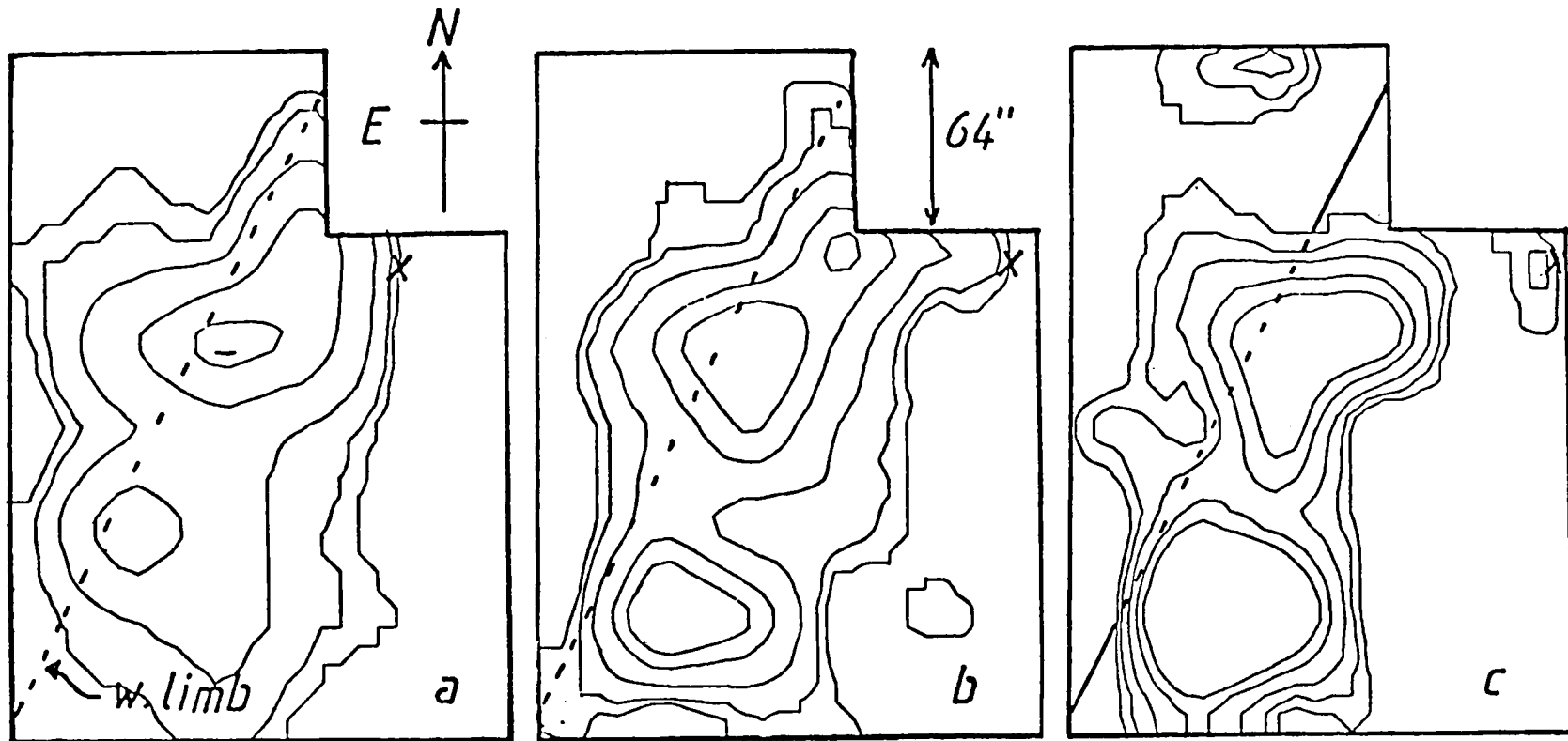


Figure 13. The X-ray transient seen in the precursor phase of the flare of 29 June. Maximum intensity contour corresponds to 0.28 counts/s. The altitudes of the three crosses are plotted in Figure 12 (labeled a, b, c).

Table 1. Average count rate per pixel, $F(k)$ in the 3.5 to 5.5 keV energy band for various exponents k in equation $F(k) = 2^{k/2} F_B$, where F_B is the average background flux, and the integration time (n seconds) needed for a 3σ statistical significance in $nF(k)$.

k	$F(k)$ (counts s^{-1})	n for $S = 3.0 \sigma$. This corresponds (s) in coarse FOV to
1	0.00645	3368 ~limit of detection
2	0.00912	1974
3	0.0129	1191 $\sim 10^{-4}$ a flare count
4	0.0182	740
6	0.0365	308
8	0.0730	139
10	0.146	65.5 $\sim 10^{-3}$ a flare count
15	0.825	11.0
20	4.67	1.93
25	26.4	Subflare
30	149.4	Flare
35	845	Major flare

Table 2. Size of the new source at 21:13:19 UT for various electron densities

η_e	Volume	Radius (if source spherical)
10^9 cm^{-3}	$3.4 \times 10^{27} \text{ cm}^3$	9330 km
10^{10}	3.4×10^{25}	2010 km
10^{11}	3.4×10^{23}	430 km
10^{12}	3.4×10^{21}	90 km

Table 3. Physical parameters of the post-flare arch revived at 14:45 on 6 November 1980.

14:09 UT	PREFLARE:	$T_{2/1} = 7.2 \times 10^6 \text{K}$ $n_e = 6.8 \times 10^8 \text{cm}^{-3}$
14:44 UT	FLARE ONSET	
15:47 UT	MAX. TEMPERATURE	$T_{2/1} = 14.0 \times 10^6 \text{K}$
17:25 UT	MAX. ENERGY DENSITY	11.2erg cm^{-3}
18:05 UT	MAX. DENSITY	$n_e = 2.4 \times 10^9 \text{cm}^{-3}$
	TOTAL VOLUME	$1.1 \times 10^{30} \text{cm}^3$
	MAX. ENERGY CONTENT	$1.2 \times 10^{31} \text{erg}$
	TOTAL MASS	$4.4 \times 10^{15} \text{g}$